Strong mechanical squeezing and optomechanical entanglement in a dissipative double-cavity system via pump modulation

Wen-Jie Zhang,[1,2] Yuchi Zhang,[1,2] Qi Guo,[1,2,*] A-Peng Liu,[3] Gang Li,[1,2] and Tiancai Zhang[1,2,†]

[1]*State Key Laboratory of Quantum Optics and Quantum Optics Devices, Institute of Opto-Electronics, College of Physics and Electronic Engineering, Shanxi University, Taiyuan, Shanxi 030006, China*

[2]*Collaborative Innovation Center of Extreme Optics, Shanxi University, Taiyuan 030006, China*

[3]*Shanxi Institute of Technology, Yangquan 045000, China*

(Received 19 July 2021; accepted 20 October 2021; published 2 November 2021)

We consider a dissipative cavity optomechanical system which couples to an auxiliary cavity with a high-quality factor and is driven by an amplitude-modulated laser field. Due to the introduction of the auxiliary cavity, we find that the steady-state mechanical squeezing can be enhanced compared to the case without an auxiliary cavity and the so-called 3 dB limit can also be broken in the resolved-sideband regime. Moreover, the squeezing can also be achieved even in the unresolved-sideband regime. We study the optomechanical entanglement in the presented system. It is found that the enhanced entanglement can be obtained by introducing the auxiliary cavity, and the entanglement can also be generated in the unresolved-sideband regime for appropriate system parameters. Numerical results show that the presented schemes have strong robustness against the thermal noise acting on the mechanical mode.

DOI: 10.1103/PhysRevA.104.053506

I. INTRODUCTION

The preparation of nonclassical states of macroscopic objects, especially entangled states and squeezed states, not only contributes to revealing the essence of nonclassical phenomena in the transition from the quantum world to the classical world, but also plays an important role in quantum computation, quantum information processing [1–3], and quantum ultra-high-precision measurements [4,5]. Optomechanical systems that exhibit nonlinear properties by the radiation pressure of light exerting on a movable mirror can be equivalent to the nonlinear optical Kerr medium [6] and provide a brilliant platform for the generation of macroscopic nonclassical states, such as the entanglement between optical and mechanical modes [7–10] and between two mechanical modes [11–21], the squeezing of a mechanical mode [22–30], etc. In general, the steady-state entanglement [7,8] and squeezing [22–24] can be obtained in optomechanical systems by radiation pressure or combining quantum measurement and feedback control. Recently, more and more methods have been proposed to prepare entanglement [9–21] and squeezing [25–30] in optomechanical systems.

In parallel with the development of cavity optomechanics, open quantum systems driven periodically by an external field have attracted much attention due to rich quantum properties and dynamical behaviors [31–33]. Especially, it was found that the amount of entanglement and squeezing can be significantly enhanced in an optomechanical system by the periodic modulation without feedback [18,24,34–43]. Mari and Eisert showed that larger degrees of mechanical squeezing and optomechanical entanglement can be generated by periodically modulating the amplitude of driving field in a standard optomechanical system [34]. Farace and Giovannetti proposed that the desired quantum effects can be enhanced or eliminated by showing an interference pattern for different relative phases between the modulations of mechanical frequency and external laser intensity [38]. Recently, Chakraborty and Sarma demonstrated that the robust mechanical entanglement can be generated by modulating external driving field and coupling strength between two mechanical oscillators [39]. The prerequisite of these schemes is the ground-state cooling of mechanical oscillator, which is usually achieved by sideband cooling. However, the realization of sideband cooling requires the system to be in the resolved-sideband regime, which is still difficult for the standard cavity optomechanical system in some experiments. An effective and easy implementation scheme is to achieve self-cooling in the unresolved-sideband regime by combining auxiliary systems. So far, many auxiliary systems have been introduced in a standard optomechanical system to cooling mechanical oscillator, such as a single atom [44–46], an atomic ensemble [43,47,48], a cavity [49], even an oscillator [50,51].

Motivated by these works above, in this paper, we propose to directly couple an auxiliary cavity with a high-quality factor to a dissipative optomechanical cavity that is driven by a periodical modulated pump. The introduction of auxiliary cavity just constructs the electromagnetically-induced-transparencylike cooling mechanism for the mechanical oscillator, which greatly reduces the requirement for the quality factor of the optomechanical cavity [49]. Combined with the periodic amplitude modulation of driving field without any feedback, it is possible to explore certifiable quantum effects

*qguo@sxu.edu.cn
†tczhang@sxu.edu.cn

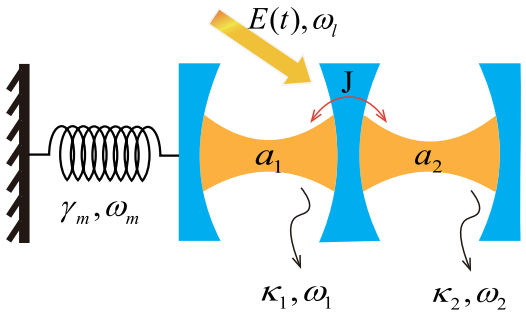

FIG. 1. Schematic diagram for the double-cavity optomechanical system. An auxiliary cavity (a_2) with a high-quality factor is directly coupled to a standard optomechanical cavity (a_1) driven by an external laser with frequency ω_l and time-dependent amplitude $E(t)$. The frequency and decay rate of mechanical oscillator are ω_m and γ_m, respectively. $\omega_{1(2)}$ and $\kappa_{1(2)}$ represent the frequency and decay rate of the two cavities. J: the cavity-cavity coupling strength.

involving macroscopic mechanical modes. We study the effect of auxiliary cavity on mechanical squeezing and optomechanical entanglement for the standard optomechanical cavity in the resolved-sideband and unresolved-sideband regimes. It is found that, in the resolved-sideband regime, the mechanical squeezing can be significantly enhanced and break the so-called 3 dB limit, and the optomechanical entanglement can also be significantly enhanced. what's more, even in the unresolved-sideband regime, the mechanical squeezing and optomechanical entanglement can also be generated. And the presented schemes have strong robustness against the thermal noise acting on the mechanical mode.

This paper is organized as follows. In Sec. II, we describe the presented model in detail and obtain the linearized dynamical equation of the system. In Sec. III, we derive the analytical solutions of the first moments for the system operators by a perturbation method, and analyze numerically and analytically the dynamical characters of the first moments. Then we derive the evolution equation of the covariance matrix (CM) describing the dynamics of the quantum fluctuations in Sec. IV. In Sec. V, we show that the enhancement and generation of mechanical squeezing in the resolved-sideband and unresolved-sideband regime, respectively. In Sec. VI, we study the optomechanical entanglement in both the resolved-sideband regime and unresolved-sideband regime. Finally, conclusions are presented in Sec. VII.

II. DESCRIPTION OF THE MODEL

The system we considered is shown in Fig. 1, in which an auxiliary cavity with a high-quality factor is directly coupled to the standard optomechanical system consisting of a movable mirror and a dissipative cavity driven by an external laser with frequency ω_l and time-dependent amplitude $E(t)$. We assume that both cavities are single-mode cavities and the cavity-cavity coupling strength is J. The movable mirror is modeled as a mechanical oscillator with frequency ω_m and decay rate γ_m. The total Hamiltonian of the system (in the unit of $\hbar = 1$) is given by

$$H = \omega_1 a_1^\dagger a_1 + \omega_2 a_2^\dagger a_2 + \frac{\omega_m}{2}(q^2+p^2) - g a_1^\dagger a_1 q + J(a_1^\dagger a_2 + a_1 a_2^\dagger) + i[E(t) a_1^\dagger e^{-i\omega_l t} - E^*(t) a_1 e^{i\omega_l t}]. \tag{1}$$

Here, a_1 ($a_1^\dagger$) and a_2 ($a_2^\dagger$) are the annihilation (creation) operators of the two cavity modes with frequency ω_1, ω_2 and decay rate κ_1, κ_2, respectively; q and p are dimensionless position and momentum operators of the mechanical mode with standard canonical commutation relation $[q\ , p] = i$; g is the single-photon optomechanical coupling coefficient. The amplitude of the external laser $E(t)$ is periodically modulated with the period τ $[E(t) = E(t+\tau)]$. In the frame rotating at the laser frequency ω_l, the Hamiltonian becomes

$$H = \delta_1 a_1^\dagger a_1 + \Delta_2 a_2^\dagger a_2 + \frac{\omega_m}{2}(q^2+p^2) - g a_1^\dagger a_1 q + J(a_1^\dagger a_2 + a_1 a_2^\dagger) + i[E(t) a_1^\dagger - E^*(t) a_1], \tag{2}$$

where $\delta_1 = \omega_1 - \omega_l$ and $\Delta_2 = \omega_2 - \omega_l$ are the detunings of two cavities with respect to the driving laser, respectively.

Aside from the unitary dynamics, the influence of the environment on the quantum system is also crucial. Therefore, taking the mechanical damping and cavity decay into account, the dissipative dynamics of the open system can be described by the following set of nonlinear quantum Langevin equations (QLEs) [52]

$$\begin{aligned}
\dot{q} &= \omega_m p, \\
\dot{p} &= -\omega_m q - \gamma_m p + g a_1^\dagger a_1 + \xi(t), \\
\dot{a}_1 &= -(\kappa_1 + i\delta_1) a_1 + i g a_1 q - i J a_2 + E(t) + \sqrt{2\kappa_1} a_1^{\rm in}(t), \\
\dot{a}_2 &= -(\kappa_2 + i\Delta_2) a_2 - i J a_1 + \sqrt{2\kappa_2} a_2^{\rm in}(t),
\end{aligned} \tag{3}$$

where $a_1^{\rm in}$ and $a_2^{\rm in}$ are zero-mean noise operators of two cavities with the correlation functions [52]

$$\begin{aligned}
\langle a_j^{\rm in}(t) a_j^{\rm in\dagger}(t')\rangle &= (n_{aj}+1)\delta(t-t'), \\
\langle a_j^{\rm in\dagger}(t) a_j^{\rm in}(t')\rangle &= n_{aj}\delta(t-t'),
\end{aligned} \tag{4}$$

where $j = 1, 2$; $n_{aj} = [\exp(\hbar\omega_j/k_B T) - 1]^{-1}$ is the mean bath photon number at the environmental temperature T, and k_B is the Boltzmann constant. $\xi(t)$ is zero-mean Brownian motion noise operator with non-Markovian correlation function [53,54]

$$\langle \xi(t)\xi(t')\rangle = \frac{\gamma_m}{2\pi\omega_m}\int \left[\coth\left(\frac{\hbar\omega}{2k_B T} + 1\right)\right]\omega e^{-i\omega(t-t')} d\omega. \tag{5}$$

For the case that the mechanical oscillator has a high-quality factor $\mathcal{Q} = \omega_m/\gamma_m \gg 1$, the above correlation function of $\xi(t)$ can be described by Markovian approximation as

$$\langle \xi(t)\xi(t') + \xi(t')\xi(t)\rangle/2 \simeq \gamma_m(2n_m+1)\delta(t-t'), \tag{6}$$

where $n_m = [\exp(\hbar\omega_m/k_B T) - 1]^{-1}$ is the mean thermal phonon number.

The QLEs in Eq. (3) are nonlinear inhomogeneous differential equations, which are usually difficult to solve directly.

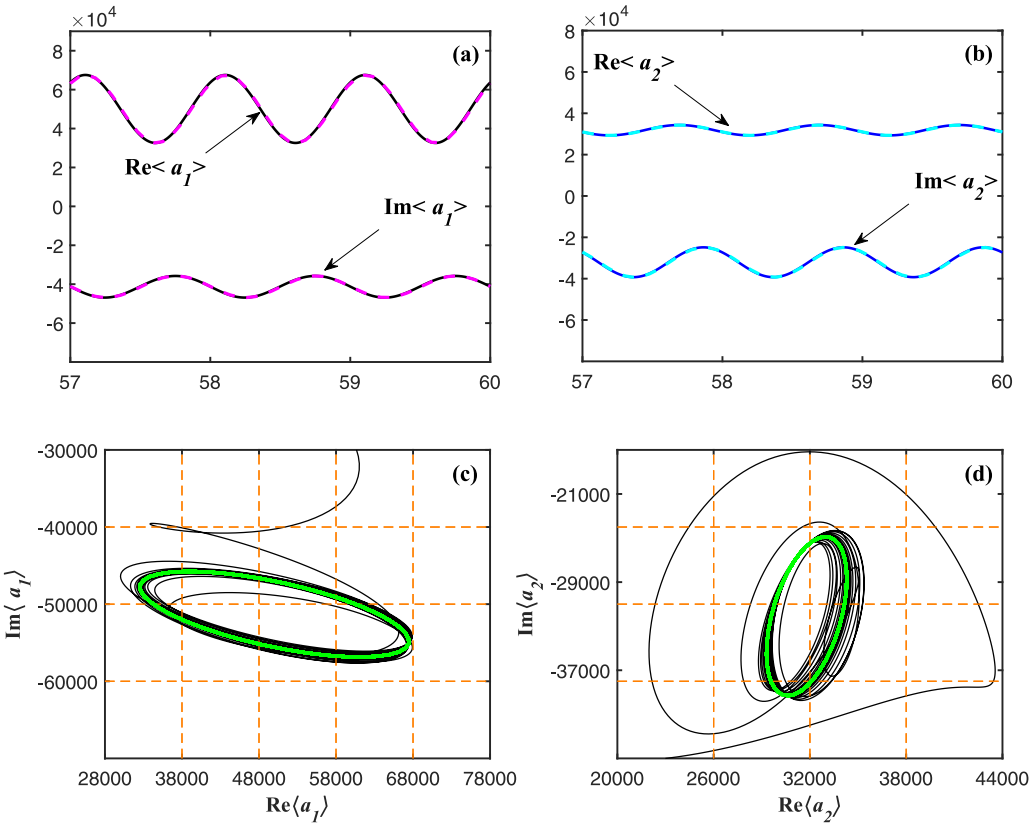

FIG. 2. Time evolution of the real part and the imaginary part of the first moments $\langle a_1(t)\rangle$ (a) and $\langle a_2(t)\rangle$ (b) during the three modulation periods $[57\tau, 60\tau]$. The dashed and solid lines represent the approximate analytical results and the exact numerical results, respectively, in both (a) and (b). (c), (d) The phase-space trajectories of $\langle a_1(t)\rangle$ and $\langle a_2(t)\rangle$ for time intervals $[0, 60\tau]$. The green (light gray) and black solid lines represent the approximate analytical results and the exact numerical results respectively in both (c) and (d). The chosen system parameters are (in units of ω_m) $\kappa_1 = 1.5$, $\delta_1 = 1$, $g = 7 \times 10^{-6}$, $\gamma_m = 10^{-5}$, $\kappa_2 = 0.1$, $\Delta_2 = -1$, $J = 0.7$, $n_m = 0$, $E_0 = 1.3 \times 10^5$, $E_{\pm 1} = 2 \times 10^4$, and $\Omega = 2$.

However, in the case of strong driving, each Heisenberg operator can be rewritten as $O = \langle O(t)\rangle + \delta O$ $(O = q, p, a_j)$, where δO is zero-mean quantum fluctuation operator around the classical c-number first moments $\langle O(t)\rangle$. Therefore, by applying the standard linearization technique to the QLEs in Eq. (3), the evolution equation of the first moments can be obtained

$$\begin{aligned}
\langle \dot{q}(t)\rangle &= \omega_m \langle p(t)\rangle,\\
\langle \dot{p}(t)\rangle &= -\omega_m \langle q(t)\rangle - \gamma_m \langle p(t)\rangle + g|\langle a_1(t)\rangle|^2,\\
\langle \dot{a}_1(t)\rangle &= -(\kappa_1 + i\delta_1)\langle a_1(t)\rangle + ig\langle a_1(t)\rangle\langle q(t)\rangle\\
&\quad - iJ\langle a_2(t)\rangle + E(t),\\
\langle \dot{a}_2(t)\rangle &= -(\kappa_2 + i\Delta_2)\langle a_2(t)\rangle - iJ\langle a_1(t)\rangle,
\end{aligned} \tag{7}$$

and the linearized QLEs of the quantum fluctuation operators are

$$\begin{aligned}
\frac{d\delta q}{dt} &= \omega_m \delta p,\\
\frac{d\delta p}{dt} &= -\omega_m \delta q - \gamma_m \delta p + g\langle a_1(t)\rangle^* \delta a_1\\
&\quad + g\langle a_1(t)\rangle \delta a_1^\dagger + \xi(t),\\
\frac{d\delta a_1}{dt} &= -(\kappa_1 + i\delta_1)\delta a_1 + ig\langle q(t)\rangle \delta a_1\\
&\quad + ig\langle a_1(t)\rangle \delta q - iJ\delta a_2 + \sqrt{2\kappa_1}a_1^{\rm in}(t),\\
\frac{d\delta a_2}{dt} &= -(\kappa_2 + i\Delta_2)\delta a_2 - iJ\delta a_1 + \sqrt{2\kappa_2}a_2^{\rm in}(t).
\end{aligned} \tag{8}$$

From the linearized QLEs above, one can obtain the corresponding linearized system Hamiltonian

$$\begin{aligned}
H^{\rm lin} &= [\delta_1 - g\langle q(t)\rangle]\delta a_1^\dagger \delta a_1 + \Delta_2 \delta a_2^\dagger \delta a_2 + \frac{\omega_m}{2}(\delta q^2 + \delta p^2)\\
&\quad + J(\delta a_2^\dagger \delta a_1 + \delta a_2 \delta a_1^\dagger) - g[\langle a_1(t)\rangle^* \delta a_1\\
&\quad + \langle a_1(t)\rangle \delta a_1^\dagger]\delta q.
\end{aligned} \tag{9}$$

III. DYNAMIC CHARACTERS OF THE FIRST MOMENTS

The time evolution of the first moments reflects the classical dynamic characters of the system. On the other hand, the time-dependent first moments are crucial for studying the dynamics of the quantum fluctuations, which can be seen from Eq. (8). Therefore, a detailed description of the first moments is necessary. Generally, it is difficult to find the exact solutions of the first moments directly. But, when the system is far away from optomechanical instabilities and multistabilities [55],

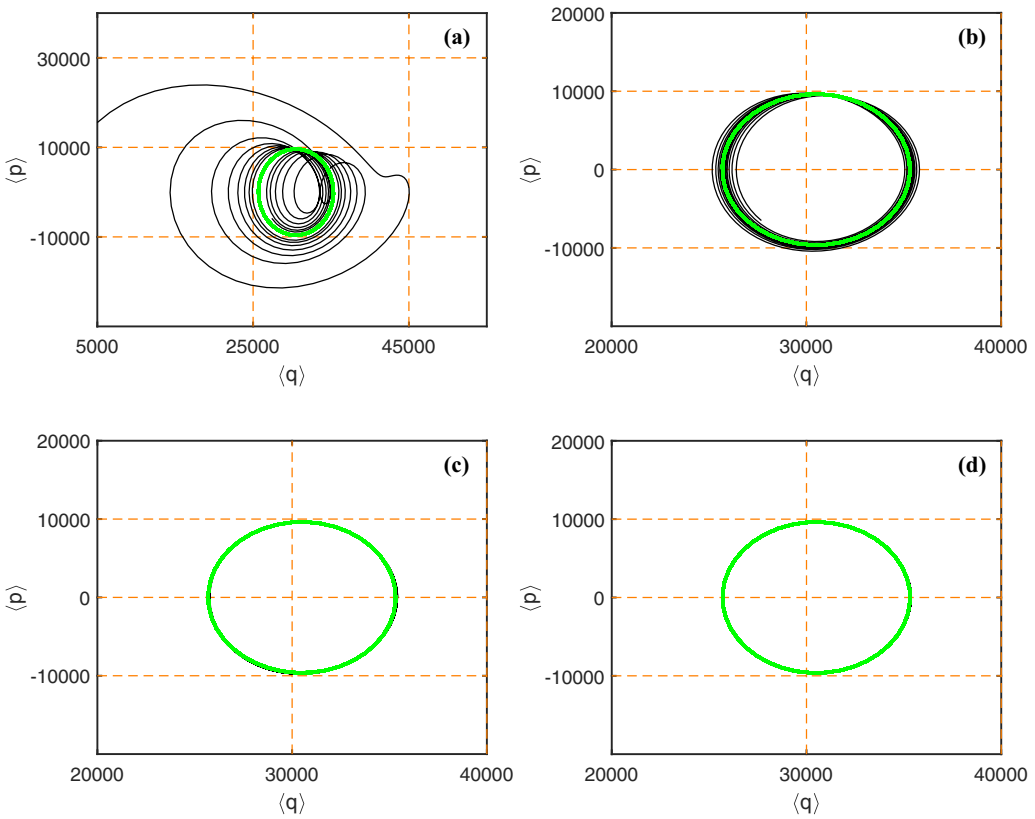

FIG. 3. The phase-space trajectories of $\langle q(t)\rangle$ and $\langle p(t)\rangle$ for the time intervals (a) $[0, 15\tau]$, (b) $[15\tau, 30\tau]$, (c) $[30\tau, 45\tau]$, and (d) $[45\tau, 60\tau]$. From (a) to (d), the green (light gray) lines and black solid lines are obtained from the approximate analytical results and the exact numerical results, respectively. The chosen parameters are the same as those in Fig. 2.

we can regard the optomechanical coupling as a perturbation term. Moreover, the asymptotic solution of first moments will have the same period as the amplitude modulation according to the Floquets theory, i.e., $\langle O(t+\tau)\rangle = \langle O(t)\rangle$. Hence, we can explore the system's asymptotic behaviors by the approximate analytical solutions and the exact numerical solutions of the first moments. To find the approximate solutions, we first perform a double expansion for $\langle O(t)\rangle$ in power series of the coupling constant g and Fourier series

$$\langle O(t)\rangle = \sum_{l=0}^{\infty}\sum_{n=-\infty}^{\infty} O_{n,l}e^{in\Omega t}g^l, \tag{10}$$

where $\Omega = 2\pi/\tau$ is the fundamental modulation frequency. In addition, Fourier series expansion can also perform on the periodically modulated amplitude $E(t)$

$$E(t) = \sum_{n=-\infty}^{\infty} E_n e^{-in\Omega t}. \tag{11}$$

Substituting Eqs. (10) and (11) into Eq. (7), the time-independent coefficients $O_{n,l}$ can be calculated by the following recursive relations

$$\begin{aligned}
&p_{n,0} = q_{n,0} = 0,\\
&a_1^{n,0} = \frac{[\kappa_2 + i(n\Omega+\Delta_2)]E_{-n}}{[\kappa_1 + i(n\Omega+\delta_1)][\kappa_2 + i(n\Omega+\Delta_2)] + J^2},\\
&a_2^{n,0} = \frac{JE_{-n}}{i[\kappa_1 + i(n\Omega+\delta_1)][\kappa_2 + i(n\Omega+\Delta_2)] + iJ^2},
\end{aligned} \tag{12}$$

which corresponds to the case of $l = 0$. When $l \geqslant 1$, we get

$$\begin{aligned}
p_{n,l} &= \frac{in\Omega}{\omega_m}q_{n,l},\\
q_{n,l} &= \omega_m\sum_{k=0}^{l-1}\sum_{m=-\infty}^{\infty}\frac{a_1^{m,k*}a_1^{n+m,l-k-1}}{\omega_m^2 - (n\Omega)^2 + i\gamma_m n\Omega},\\
a_1^{n,l} &= i[\kappa_2 + i(n\Omega+\Delta_2)]\\
&\quad\times\sum_{k=0}^{l-1}\sum_{m=-\infty}^{\infty}\frac{a_1^{m,k}q_{n-m,l-k-1}}{[\kappa_1+i(n\Omega+\delta_1)][\kappa_2+i(n\Omega+\Delta_2)]+J^2},\\
a_2^{n,l} &= J\sum_{k=0}^{l-1}\sum_{m=-\infty}^{\infty}\frac{a_1^{m,k}q_{n-m,l-k-1}}{[\kappa_1+i(n\Omega+\delta_1)][\kappa_2+i(n\Omega+\Delta_2)]+J^2}.
\end{aligned} \tag{13}$$

Now, in order to obtain the approximate analytical solutions, we truncate the series above to $l \leqslant 6$ and $|n| \leqslant 5$, and truncate the series of the modulated amplitude $E(t)$ to $|n| \leqslant 1$, that is, the time-dependent amplitude takes the form of $E(t) = E_{-1}e^{i\Omega t} + E_0 + E_1e^{-i\Omega t}$. Then we plot the time evolution and phase-space trajectories of the first moments $\langle a_1(t)\rangle$ and $\langle a_2(t)\rangle$ in Fig. 2 to analyze the dynamics of the cavity modes by using both numerical and analytical results. Figures 2(a) and 2(b) show the asymptotic periodic evolution of the real and imaginary parts of the first moments $\langle a_1(t)\rangle$ and $\langle a_2(t)\rangle$, respectively, from which it can be seen that the

evolution period of the first moments is indeed the same as the modulation period τ in the long-time limit. Furthermore, we find that the approximate analytical solutions (dashed lines) in Eqs. (12) and (13) agree well with the exact numerical solutions (solid lines) obtained from Eq. (7) after about 60 modulation periods, which further verifies the accuracy of the analytical solutions by perturbation approximation. In order to show the dynamics of the system more clearly, Figs. 2(c) and 2(d) exhibit the phase-space trajectories of $\langle a_1(t)\rangle$ and $\langle a_2(t)\rangle$, respectively, in which the green (light gray) and black solid lines, respectively, represent the approximate analytical results and the exact numerical results. As mentioned above, both trajectories from the numerical results converge to a limit cycle agreed well with the analytical results after about 60 modulation periods. To further show the convergence process, we plot the phase-space trajectories of $\langle p(t)\rangle$ and $\langle q(t)\rangle$ in different time periods in Fig. 3. From Figs. 3(a) to 3(d), we can clearly observe the slow asymptotic process of the accurate numerical results and the analytical results.

IV. DYNAMICS OF QUANTUM FLUCTUATIONS

After obtaining the evolution characteristic of the first moments, we can easily solve the quantum fluctuations dynamics of the system. To this effect, we introduce the quadrature operators of the two cavity modes and the corresponding input noise operators

$$\begin{aligned}
\delta x_1 &= \frac{\delta a_1 + \delta a_1^\dagger}{\sqrt{2}}, \quad \delta y_1 = \frac{\delta a_1 - \delta a_1^\dagger}{i\sqrt{2}},\\
\delta x_2 &= \frac{\delta a_2 + \delta a_2^\dagger}{\sqrt{2}}, \quad \delta y_2 = \frac{\delta a_2 - \delta a_2^\dagger}{i\sqrt{2}},\\
x_1^{\rm in} &= \frac{a_1^{\rm in} + a_1^{\rm in\dagger}}{\sqrt{2}}, \quad y_1^{\rm in} = \frac{a_1^{\rm in} - a_1^{\rm in\dagger}}{i\sqrt{2}},\\
x_2^{\rm in} &= \frac{a_2^{\rm in} + a_2^{\rm in\dagger}}{\sqrt{2}}, \quad y_2^{\rm in} = \frac{a_2^{\rm in} - a_2^{\rm in\dagger}}{i\sqrt{2}},
\end{aligned} \tag{14}$$

and all the quadrature operators and corresponding noise operators can be expressed as the column vectors

$$\begin{aligned}
u(t) &= [\delta q, \delta p, \delta x_1, \delta y_1, \delta x_2, \delta y_2]^T,\\
n(t) &= [0, \xi(t), \sqrt{2\kappa_1}x_1^{\rm in}(t), \sqrt{2\kappa_1}y_1^{\rm in}(t),\\
&\quad \sqrt{2\kappa_2}x_2^{\rm in}(t), \sqrt{2\kappa_2}y_2^{\rm in}(t)]^T.
\end{aligned} \tag{15}$$

Then, the linearized QLEs of the quantum fluctuations in Eq. (8) can be rewritten as

$$\frac{du}{dt} = R(t)u + n(t), \tag{16}$$

where $R(t)$ is a 6×6 time-dependent matrix

$$R(t) = \begin{bmatrix}
0 & \omega_m & 0 & 0 & 0 & 0\\
-\omega_m & -\gamma_m & G_x(t) & G_y(t) & 0 & 0\\
-G_y(t) & 0 & -\kappa_1 & \Delta_1(t) & 0 & J\\
G_x(t) & 0 & -\Delta_1(t) & -\kappa_1 & -J & 0\\
0 & 0 & 0 & J & -\kappa_2 & \Delta_2\\
0 & 0 & -J & 0 & -\Delta_2 & -\kappa_2
\end{bmatrix}, \tag{17}$$

where

$$\Delta_1(t) = \delta_1 - g\langle q(t)\rangle \tag{18}$$

is the effective time-modulated detuning; $G_x(t)$ and $G_y(t)$, respectively, are the real and imaginary parts of the effective coupling strength

$$G(t) = \sqrt{2}g\langle a_1(t)\rangle. \tag{19}$$

When the system is stable, due to the linearized process of fluctuations evolution and the zero-mean Gaussian nature of the noises, the asymptotic quantum state of the system will evolve into a Gaussian state and is independent of the initial states [56]. Here, the initial states of the cavity modes (a_1 and a_2) are prepared in vacuum state while the mechanical mode is initially in the thermal state in equilibrium with mechanical bath. The asymptotic state of the fluctuations can be characterized by the covariance matrix $\sigma(t)$, whose elements are defined as

$$\sigma_{k,l} = \langle u_k(t)u_l(t) + u_l(t)u_k(t)\rangle/2. \tag{20}$$

We can derive the motion equation of the CM $\sigma(t)$ according to Eqs. (16) and (20)

$$\frac{d\sigma}{dt} = R(t)\sigma(t) + \sigma(t)R(t)^T + D, \tag{21}$$

where $R(t)^T$ denotes the transpose of $R(t)$; D is a diffusion matrix whose elements are related to noise correlation functions and defined as

$$\delta(t-t')D_{k,l} = \langle n_k(t)n_l(t') + n_l(t')n_k(t)\rangle/2. \tag{22}$$

From Eqs. (4) and (6), we find that D is a diagonal matrix

$$\begin{aligned}
D = {\rm diag}[0,\ &\gamma_m(2n_m+1), \kappa_1(2n_{a1}+1), \kappa_1(2n_{a1}+1),\\
&\kappa_2(2n_{a2}+1), \kappa_2(2n_{a2}+1)].
\end{aligned} \tag{23}$$

Due to the periodicity of the elements of $R(t)$ in Eq. (17), the solutions of linear differential equation (21) will have the same periodicity as $R(t)$ in a long-time limit according to the Floquet's theorem

$$\sigma(t) = \sigma(t+\tau). \tag{24}$$

Now, the dynamic evolution of quantum fluctuations is completely described based on the evolution equation of the CM $\sigma(t)$. In the following calculations, all eigenvalues of $R(t)$ have a negative real part for all time to ensure the stability of the system, which is justified according to the Routh-Hurwitz criterion [57].

V. MECHANICAL SQUEEZING IN THE RESOLVED-SIDEBAND AND UNRESOLVED-SIDEBAND REGIMES

We now investigate the generation of mechanical squeezing when the auxiliary cavity is directly coupled to the optomechanical cavity. Because of the zero mean of the quantum fluctuations, the first and second diagonal elements of the CM $\sigma(t)$ represent the variance of position and momentum operators of the mechanical oscillator, respectively. According to the Heisenberg uncertainty principle and commutative relation $[q, p] = i$, as long as the variance $V(q)$ or $V(p)$, i.e.,

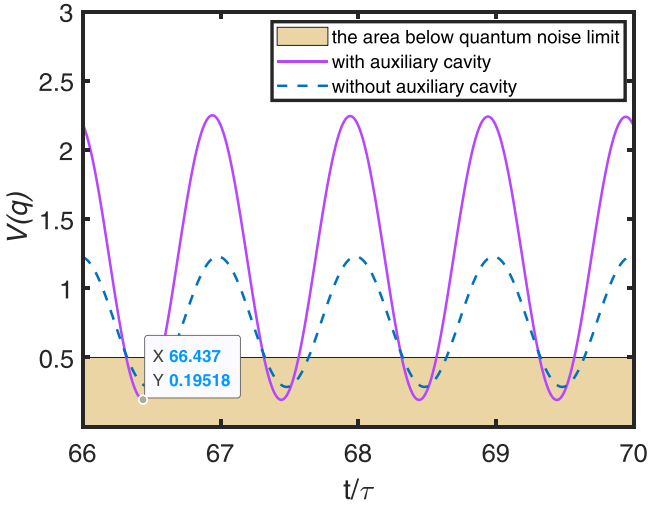

FIG. 4. Variance of the position operator of the mechanical oscillator in the resolved-sideband regime. The solid and dashed lines correspond to the cases with and without auxiliary cavity, respectively. The rectangular colored region represents the area below quantum noise limit. All the selected parameters except those related to the auxiliary cavity are the same as in Ref. [34]. The parameters related to the auxiliary cavity are (in units of ω_m) $\kappa_2 = 0.01$, $\Delta_2 = -1.1$, $J = 0.6$.

the first or second diagonal elements of the CM $\sigma(t)$, is less than $\frac{1}{2}$, it can be judged that mechanical squeezing has been generated.

In order to exhibit the behavior of mechanical squeezing, we first plot the asymptotic evolution of the position variance of the mechanical oscillator from $t = 66\tau$ to 70τ in the resolved-sideband regime ($\kappa_1 < \omega_m$) in Fig. 4, in which the solid line is the variance in the presented scheme, and the dashed line is the one in Ref. [34], i.e., the case without the auxiliary cavity. It can be seen from Fig. 4 that the position quadrature of the mechanical oscillator is periodically squeezed with the same period as the amplitude modulation. what's more, the squeezing can be enhanced compared with the scheme in Ref. [34] and broke the so-called 3 dB limit in schemes based on the parametric interaction [22–24,58], which are limited by a factor of $\frac{1}{2}$ below the zero-point level, i.e., 0.25. For example, $V(q) = 0.195\,18$ for $t = 66.437\tau$. This means that strong mechanical squeezing can be achieved by coupling an auxiliary cavity to a resolved-sideband optomechanical system. For the case that the optomechanical cavity is in the unresolved-sideband regime, by choosing appropriate system parameters, the mechanical squeezing can also be achieved as shown in Fig. 5(a). Moreover, Fig. 5(b) shows that the mechanical squeezing can still be generated even when the mean thermal phonon number $n_m = 3000$ (corresponding to the environmental temperature $T = 0.144$ K), which proves that the presented scheme for mechanical squeezing is robust against the noise from the mechanical thermal reservoir.

What needs to be pointed out is that the steady-state squeezing can be achieved after a long period of time, and the periodicity in Figs. 4 and 5 is just the periodicity of the squeezing direction in the phase space. In order to show the characteristic of the mechanical squeezing more comprehensively, we depict the Wigner functions [56] in the phase space at different specific moments in two contiguous periods $[68\tau, 70\tau]$ and the evolution of single-mode squeezing parameter r in Figs. 6 and 7, respectively, where the squeezing parameter r is defined as the logarithm of the minimum eigenvalue of the CM $\sigma(t)$ [34,43]. It can be seen from Fig. 6 that the shapes of the Wigner functions at the same moments in the two modulation periods are identical, which further demonstrates the dynamical behavior of the system has the same period as the amplitude modulation. During every period, the squeezing direction rotates once in the phase space, but the degree of squeezing remains the same and this is because the squeezing parameter will be a constant in long-time limit as shown in Fig. 7.

The realization of many macroscopic quantum effects in an optomechanical system, especially mechanical squeezing, must cool the mechanical oscillator to the ground state at first. In our scheme, the introduction of the auxiliary cavity and the periodic modulation of driving field are the key factors

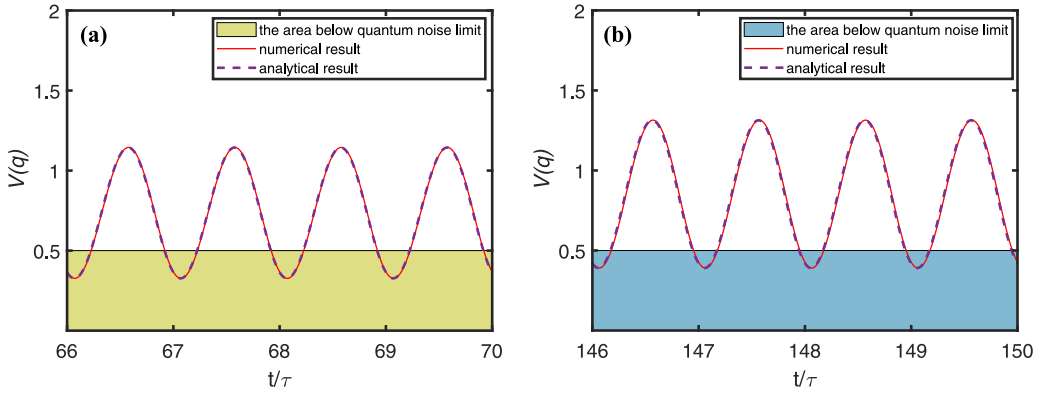

FIG. 5. Variance of the position operator of the mechanical oscillator in the unresolved-sideband regime with the mean thermal phonon number (a) $n_m = 0$ and (b) $n_m = 3000$. The dashed and solid lines correspond to the analytical solutions and the exact numerical results of first moments, respectively. The rectangular colored regions represent the area below quantum noise limit. The chosen system parameters are (in units of ω_m) $\kappa_1 = 5$, $\delta_1 = 1$, $g = 8 \times 10^{-5}$, $\gamma_m = 10^{-6}$, $\kappa_2 = 0.01$, $\Delta_2 = -1$, $J = 4$, $E_0 = 1.5 \times 10^5$, $E_{\pm 1} = 2 \times 10^4$, and $\Omega = 2$.

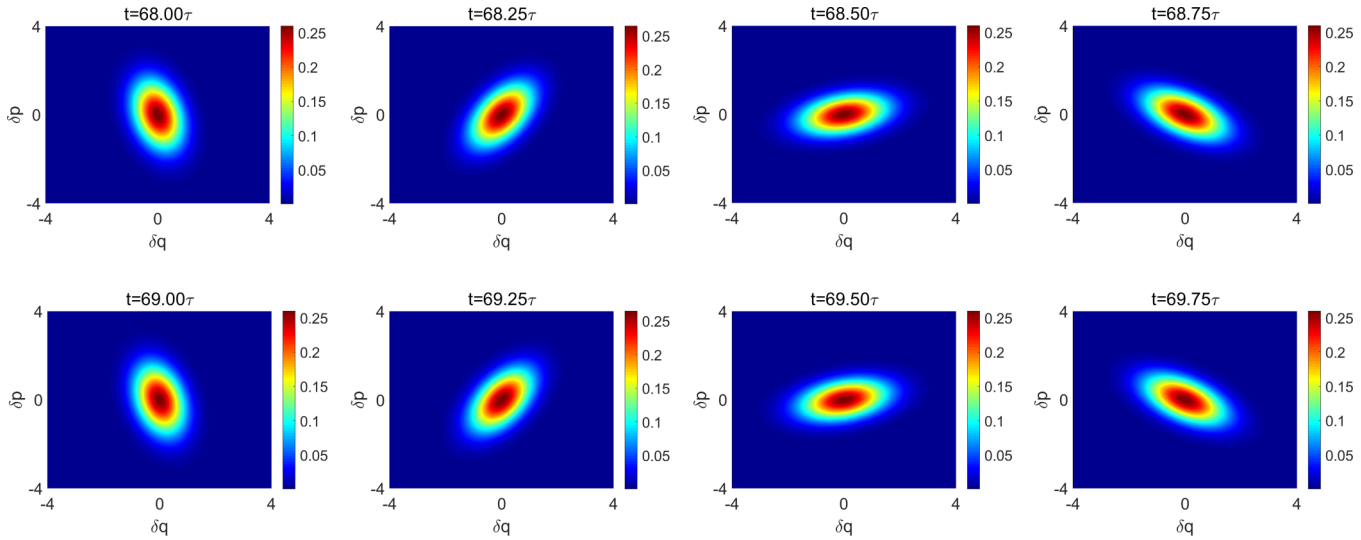

FIG. 6. Wigner functions of the mechanical mode at some specific times. The chosen parameters are the same as those in Fig. 5.

for mechanical squeezing. The precooling process has not been performed in the presented scheme, which is owed to the self-cooling mechanism induced by the auxiliary cavity. In Ref. [49], it has been demonstrated that the mechanical oscillator can be cooled to ground state in a double-cavity optomechanical system even in the unresolved-sideband regime due to the electromagnetically-induced-transparencylike effect, and that is also why the presented scheme is robust against the thermal noise of the mechanical mode. On the other hand, the generation of mechanical squeezing originates from the nonlinear effect induced by the periodic amplitude modulation, which is similar to the parametric amplification process. The amplitude of the driving field is modulated at twice mechanical mode frequency, which is equivalent to modulate the spring constant of the optical spring effect [34,38,59]. Therefore, using the presented model, the mechanical squeezing can be achieved even in the unresolved-sideband regime.

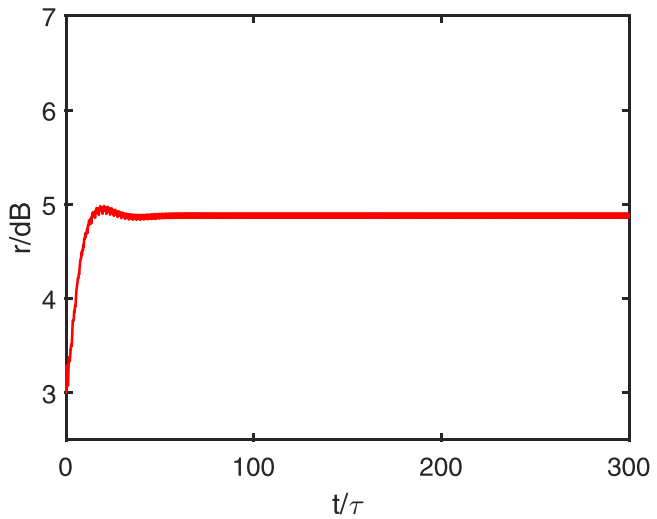

FIG. 7. Time evolution of the mechanical mode-squeezing parameter r. The chosen parameters are the same as those in Fig. 5.

VI. OPTOMECHANICAL ENTANGLEMENT IN THE RESOLVED-SIDEBAND AND UNRESOLVED-SIDEBAND REGIMES

In this section, we turn to investigate the entanglement between the optical mode and the mechanical mode in the presented system. As mentioned above, since the system's asymptotic state is Gaussian, a convenient method to measure the entanglement is the logarithmic negativity E_N [60,61], which can be readily computed from the reduced 4×4 CM $\sigma_{cm}(t)$ for one of the cavity modes and the mechanical mode. Here we focus on the entanglement between the auxiliary cavity and the movable mirror, so $\sigma_{cm}(t)$ can be gotten from the full 6×6 CM $\sigma(t)$ by extracting the first two and last two

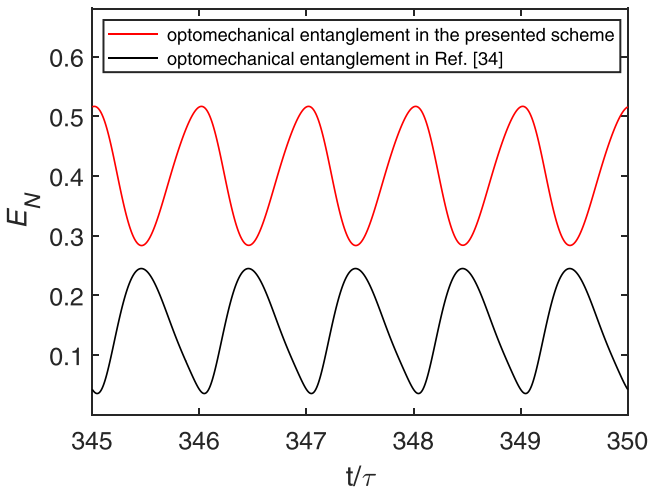

FIG. 8. Time evolution of optomechanical entanglement E_N in the resolved-sideband regime. The red (light gray) and black lines represent the optomechanical entanglement in the presented scheme and in Ref. [34], respectively. All the selected parameters except those related to the auxiliary cavity are the same as in Ref. [34]. The parameters related to the auxiliary cavity are (in units of ω_m) $\kappa_2 = 0.03$, $\Delta_2 = -0.8$, $J = 0.5$.

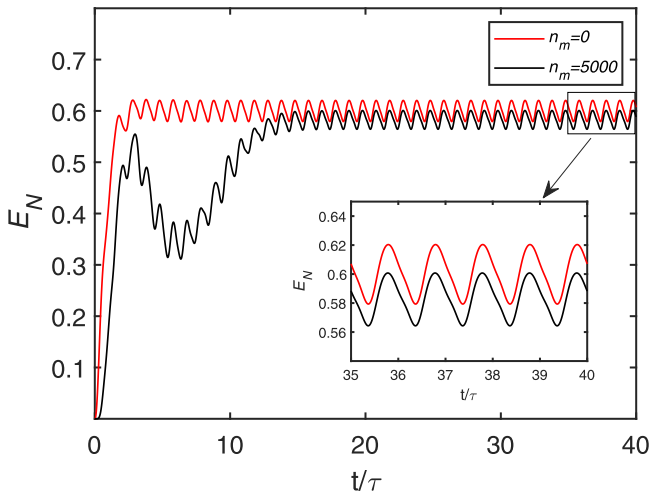

FIG. 9. Time evolution of optomechanical entanglement E_N in the unresolved-sideband regime. The red (light gray) and black lines represent the cases for the mean thermal phonon number $n_m = 0$ and 5000, respectively. The lower inset presents zooming in on the tiny rectangular area. The chosen system parameters are (in units of ω_m) $\kappa_1 = 2$, $\delta_1 = 1$, $g = 10^{-5}$, $\gamma_m = 10^{-6}$, $\kappa_2 = 0.01$, $\Delta_2 = -1$, $J = 1$, $E_0 = 2 \times 10^5$, $E_{\pm 1} = 4 \times 10^4$, and $\Omega = 2$.

rows and columns, where $\sigma(t)$ can be gotten by numerically solving Eq. (21). If we write the reduced 4×4 CM $\sigma_{cm}(t)$ as the block matrix form

$$\sigma_{cm}(t) = \begin{bmatrix} V_m & V_{cm} \\ V_{cm}^T & V_c \end{bmatrix}, \tag{25}$$

where V_m, V_c, and V_{cm} are 2×2 matrices, and E_N is given by [60,61]

$$E_N = \max[0, -\ln(2\eta^-)], \tag{26}$$

with

$$\eta^- \equiv 2^{-1/2}\{\Sigma - [\Sigma^2 - 4\det\sigma_{cm}]^{1/2}\}^{1/2},$$
$$\Sigma \equiv \det V_m + \det V_c - 2\det V_{cm}. \tag{27}$$

If $E_N > 0$, i.e., $\eta^- < \frac{1}{2}$, the cavity mode and mechanical mode are entangled.

We first numerically simulate the optomechanical entanglement dynamics between the auxiliary cavity and the mirror in Fig. 8 with the red (light gray) line, where the optomechanical cavity is in the resolved-sideband regime and all the parameters are the same as those in Ref. [34] besides the auxiliary cavity. For comparison, we also give the optomechanical entanglement in Ref. [34] (the black line in Fig. 8). Obviously, the enhanced optomechanical entanglement can be obtained by introducing the auxiliary cavity at the expense of the entanglement between the optomechanical cavity and the mirror tending to zero (not shown in Fig. 8). In addition, we note that the optomechanical entanglement has the same period as amplitude modulation after a long-time evolution. In Fig. 9, we show the process of obtaining steady-state optomechanical entanglement when the system is in the unresolved-sideband regime ($\kappa_1 > \omega_m$). It is found that the optomechanical entanglement can also be generated even in the unresolved-sideband regime, regardless of the case of the mean thermal phonon number $n_m = 0$ or 5000 (corresponding to the environmental temperature $T = 0.24$ K), which means the entanglement is robust against the thermal mechanical bath.

VII. CONCLUSIONS

In conclusion, we have studied the mechanical squeezing and optomechanical entanglement in a double-cavity optomechanical system driven by a periodically modulated laser. We analyzed the asymptotic behavior of the system dynamics by solving the first moments of the system operators numerically and analytically, and found that the period of the classical evolution of system is the same as the amplitude modulation in the long-time limit. Then, we showed that the introduction of the auxiliary cavity can enhance the mechanical squeezing in the resolved-sideband regime, and due to the self-cooling mechanism, the mechanical squeezing can be achieved even in the unresolved-sideband regime. On the other hand, after introducing the auxiliary cavity, the enhanced optomechanical entanglement can be obtained in both the resolved-sideband and the unresolved-sideband regimes. We numerically evaluated the influence of the mechanical thermal bath, which indicates that both the mechanical squeezing and optomechanical entanglement have strong robustness against the mechanical noise. Moreover, the double-cavity optomechanical system can be achieved experimentally based on Fabry-Pérot cavities or whispering-gallery cavities [62–64]. Therefore, the presented scheme may be meaningful for the ultraprecise measurement based on mechanical squeezing (e.g., the gravitational wave detection) and the exploration of the macroscopic quantum effects based on optomechanical system.

ACKNOWLEDGMENTS

This work is supported by the National Natural Science Foundation of China under Grants No. 11604190 and No. 11974223, the Natural Science Foundation of Shanxi Province Grant No. 201901D211167, the Scientific and Technological Innovation Programs of Higher Education Institutions in Shanxi Grants No. 2019L0043 and No. 2019L0988, and the Fund for Shanxi "1331 Project" Key Subjects Construction.

[1] S. Mancini, D. Vitali, and P. Tombesi, Phys. Rev. Lett. **90**, 137901 (2003).
[2] S. L. Braunstein and P. van Loock, Rev. Mod. Phys. **77**, 513 (2005).
[3] S. G. Hofer, W. Wieczorek, M. Aspelmeyer, and K. Hammerer, Phys. Rev. A **84**, 052327 (2011).
[4] M. D. LaHaye, O. Buu, B. Camarota, and K. C. Schwab, Science **304**, 74 (2004).
[5] A. Motazedifard, F. Bemani, M. H. Naderi, R. Roknizadeh, and D. Vitali, New J. Phys. **18**, 073040 (2016).
[6] S. Mancini and P. Tombesi, Phys. Rev. A **49**, 4055 (1994).

[7] D. Vitali, S. Gigan, A. Ferreira, H. R. Böhm, P. Tombesi, A. Guerreiro, V. Vedral, A. Zeilinger, and M. Aspelmeyer, Phys. Rev. Lett. **98**, 030405 (2007).

[8] L. Tian, M. S. Allman, and R. W. Simmonds, New J. Phys. **10**, 115001 (2008).

[9] C. Genes, A. Mari, P. Tombesi, and D. Vitali, Phys. Rev. A **78**, 032316 (2008).

[10] S. Barzanjeh, D. Vitali, P. Tombesi, and G. J. Milburn, Phys. Rev. A **84**, 042342 (2011).

[11] Y.-D. Wang and A. A. Clerk, Phys. Rev. Lett. **110**, 253601 (2013).

[12] S. Huang and G. S. Agarwal, New J. Phys. **11**, 103044 (2009).

[13] S. Pirandola, D. Vitali, P. Tombesi, and S. Lloyd, Phys. Rev. Lett. **97**, 150403 (2006).

[14] K. Børkje, A. Nunnenkamp, and S. M. Girvin, Phys. Rev. Lett. **107**, 123601 (2011).

[15] H. Tan, L. F. Buchmann, H. Seok, and G. Li, Phys. Rev. A **87**, 022318 (2013).

[16] J.-Q. Liao, Q.-Q. Wu, and F. Nori, Phys. Rev. A **89**, 014302 (2014).

[17] J. Li, I. M. Haghighi, N. Malossi, S. Zippilli, and D. Vitali, New J. Phys. **17**, 103037 (2015).

[18] M. Wang, X.-Y. Lu, Y.-D. Wang, J.-Q. You, and Y. Wu, Phys. Rev. A **94**, 053807 (2016).

[19] J. Li, G. Li, S. Zippilli, D. Vitali, and T. Zhang, Phys. Rev. A **95**, 043819 (2017).

[20] C.-H. Bai, D.-Y. Wang, H.-F. Wang, A.-D. Zhu, and S. Zhang, Sci. Rep. **7**, 2545 (2017).

[21] X. Y. Huang, E. Zeuthen, D. V. Vasilyev, Q. Y. He, K. Hammerer, and E. S. Polzik, Phys. Rev. Lett. **121**, 103602 (2018).

[22] M. J. Woolley, A. C. Doherty, G. J. Milburn, and K. C. Schwab, Phys. Rev. A **78**, 062303 (2008).

[23] A. Nunnenkamp, K. Børkje, J. G. E. Harris, and S. M. Girvin, Phys. Rev. A **82**, 021806(R) (2010).

[24] J.-Q. Liao and C. K. Law, Phys. Rev. A **83**, 033820 (2011).

[25] W.-J. Gu, G.-X. Li, and Y.-P. Yang, Phys. Rev. A **88**, 013835 (2013).

[26] M. Asjad, G. S. Agarwal, M. S. Kim, P. Tombesi, G. Di Giuseppe, and D. Vitali, Phys. Rev. A **89**, 023849 (2014).

[27] G. S. Agarwal and S. Huang, Phys. Rev. A **93**, 043844 (2016).

[28] X.-Y. Lü, J.-Q. Liao, L. Tian, and F. Nori, Phys. Rev. A **91**, 013834 (2015).

[29] D.-Y. Wang, C.-H. Bai, H.-F. Wang, A.-D. Zhu, and S. Zhang, Sci. Rep. **6**, 24421 (2016).

[30] D.-Y. Wang, C.-H. Bai, H.-F. Wang, A.-D. Zhu, and S. Zhang, Sci. Rep. **6**, 38559 (2016).

[31] A. Eckardt, C. Weiss, and M. Holthaus, Phys. Rev. Lett. **95**, 260404 (2005).

[32] L. Viola, E. Knill, and S. Lloyd, Phys. Rev. Lett. **82**, 2417 (1999).

[33] H. P. Breuer, M. Holthaus, and K. Dietz, Z. Phys. D **8**, 349 (1988).

[34] A. Mari and J. Eisert, Phys. Rev. Lett. **103**, 213603 (2009).

[35] R.-X. Chen, L.-T. Shen, Z.-B. Yang, H.-Z. Wu, and S.-B. Zheng, Phys. Rev. A **89**, 023843 (2014).

[36] C.-G. Liao, H. Xie, X. Shang, Z.-H. Chen, and X.-M. Lin, Opt. Express **26**, 13783 (2018).

[37] C.-S. Hu, Z.-B. Yang, H. Wu, Y. Li, and S.-B. Zheng, Phys. Rev. A **98**, 023807 (2018).

[38] A. Farace and V. Giovannetti, Phys. Rev. A **86**, 013820 (2012).

[39] S. Chakraborty and A. K. Sarma, Phys. Rev. A **97**, 022336 (2018).

[40] Y. Han, J. Cheng, and L. Zhou, Eur. Phys. J. D **67**, 20 (2013).

[41] B. Rogers, M. Paternostro, G. M. Palma, and G. De Chiara, Phys. Rev. A **86**, 042323 (2012).

[42] W.-J. Gu and G.-X. Li, Opt. Express **21**, 20423 (2013).

[43] C.-H. Bai, D.-Y. Wang, S. Zhang, S. Liu, and H.-F. Wang, Ann. Phys. (Berlin) **531**, 1800271 (2019).

[44] D. Breyer and M. Bienert, Phys. Rev. A **86**, 053819 (2012).

[45] S. Zhang, J.-Q. Zhang, J. Zhang, C.-W. Wu, W. Wu, and P.-X. Chen, Opt. Express **22**, 028118 (2014).

[46] C. Genes, H. Ritsch, M. Drewsen, and A. Dantan, Phys. Rev. A **84**, 051801(R) (2011).

[47] C. Genes, H. Ritsch, and D. Vitali, Phys. Rev. A **80**, 061803(R) (2009).

[48] R.-P. Zeng, S. Zhang, C.-W. Wu, W. Wu, and P.-X. Chen, J. Opt. Soc. Am. B **32**, 2314 (2015).

[49] Y.-J. Guo, K. Li, W.-J. Nie, and Y. Li, Phys. Rev. A **90**, 053841 (2014).

[50] Y.-X. Zhang, S. Wu, and Z.-B. Chen, and Y. Shikano, Phys. Rev. A **94**, 023823 (2016).

[51] T. Ojanen and K. Børkje, Phys. Rev. A **90**, 013824 (2014).

[52] C. W. Gardiner and P. Zoller, *Quantum Noise*, 3rd ed. (Springer, New York, 2004).

[53] V. Giovannetti and D. Vitali, Phys. Rev. A **63**, 023812 (2001).

[54] A. A. Clerk, M. H. Devoret, S. M. Girvin, F. Marquardt, and R. J. Schoelkopf, Rev. Mod. Phys. **82**, 1155 (2010).

[55] M. Ludwig, B. Kubala, and F. Marquardt, New J. Phys. **10**, 095013 (2008).

[56] C. Weedbrook, S. Pirandola, R. García-Patrón, N. J. Cerf, T. C. Ralph, J. H. Shapiro, and S. Lloyd, Rev. Mod. Phys. **84**, 621 (2012).

[57] E. X. DeJesus and C. Kaufman, Phys. Rev. A **35**, 5288 (1987).

[58] M. Schmidt, M. Ludwig, and F. Marquardt, New J. Phys. **14**, 125005 (2012).

[59] A. Kronwald, F. Marquardt, and A. A. Clerk, Phys. Rev. A **88**, 063833 (2013).

[60] G. Vidal and R. F. Werner, Phys. Rev. A **65**, 032314 (2002).

[61] G. Adesso, A. Serafini, and F. Illuminati, Phys. Rev. A **70**, 022318 (2004).

[62] I. S. Grudinin, H. Lee, O. Painter, and K. J. Vahala, Phys. Rev. Lett. **104**, 083901 (2010).

[63] B. Peng, S. K. Ozdemir, F. Lei, F. Monifi, M. Gianfreda, G. L. Long, S. Fan, F. Nori, C. M. Bender, and L. Yang, Nat. Phys. **10**, 394 (2014).

[64] H. Jing, S. K. Ozdemir, X.-Y. Lü, J. Zhang, L. Yang, and F. Nori, Phys. Rev. Lett. **113**, 053604 (2014).